Received: 28 July 2023 | Revised: 18 October 2023 | Accepted: 5 November 2023

DOI: 10.1002/jemt.24458

RESEARCH ARTICLE

MICROSCOPY RESEARCH & TECHNIQUE WILEY

The in vitro cytotoxic effects of natural (fibrous epsomite crystals) and synthetic (Epsom salt) magnesium sulfate

Sara Salucci[1] | Matteo Giordani[2] | Michele Betti[3] | Laura Valentini[3] | Pietro Gobbi[3] | Michele Mattioli[2]

[1]Department of Biomedical and NeuroMotor Sciences (DIBINEM), University of Bologna, Bologna, Italy

[2]Department of Pure and Applied Sciences, University of Urbino Carlo Bo, Urbino, Italy

[3]Department of Biomolecular Sciences (DISB), University of Urbino Carlo Bo, Urbino, Italy

Correspondence
Sara Salucci, Department of Biomedical and NeuroMotor Sciences (DIBINEM), University of Bologna, Bologna 40126, Italy.
Email: sara.salucci@unibo.it

Funding information
PRIN: PROGETTI DI RICERCA DI RILEVANTE INTERESSE NAZIONALE-Bando 2017-Prot, Grant/Award Number: 20173X8WA4

Review Editor: Alberto Diaspro

Abstract

Exposure to mineral fibers represents an occupational and environmental hazard since particulate inhalation leads to several health disorders. However, few data are available on the effect of fibers with high solubility like natural epsomite, a water-soluble fiber with an inhalable size that allows it to penetrate biological systems, with regard to the respiratory tract. This study evaluated the natural (fibrous epsomite) and synthetic (Epsom salt) magnesium sulfate pathogenicity. Investigations have been performed through morpho-functional and biochemical analyses, in an in vitro cell model that usually grows as monocytes, but that under appropriate conditions differentiates into macrophages. These latter, known as alveolar macrophages, if referred to lungs, represent the first line of defense against harmful inhaled stimuli. Morphological observations reveal that, if Epsom salt induces osmotic stress on cell culture, natural epsomite fibers lead to cellular alterations including thickening of the nuclear envelope and degenerated mitochondria. Moreover, the insoluble fraction (impurities) internalized by cells induces diffuse damage characterized at the highest dosage and exposure time by secondary necrosis or necrotic cell death features. Biochemical analyses confirm this mineral behavior that involves MAPK pathway activation, resulting in many different cellular responses ranging from proliferation control to cell death. Epsom salt leads to MAPK/ERK activation, a marker predictive of overall survival. Unlike, natural epsomite induces upregulation of MAPK/p38 protein involved in the phosphorylation of downstream targets driving necrotic cell death. These findings demonstrate natural epsomite toxicity on U937 cell culture, making the inhalation of these fibers potentially hazardous for human health.

Research Highlights

- Natural epsomite and synthetic Epsom salt effects have been evaluated in U937 cell model.
- Epsom salt induces an osmotic cellular stress.
- Natural epsomite fibers lead to cellular damage and can be considered potentially dangerous for human health.

KEYWORDS
cell death, epsomite fibers, magnesium sulfate, osmotic stress, U937 cells

1 | INTRODUCTION

Mineral dust and particles of inhalable size are subjects of concern so far due to their effect on human health. Some mineral fibers such as asbestos (chrysotile, amosite, crocidolite, asbestos anthophyllite, asbestos tremolite and asbestos actinolite) and zeolites, in particular erionite, have been extensively investigated in the last decades (e.g., Cangiotti et al., 2017, 2018; Gualtieri, 2023; World Health Organization, 1986; Thompson et al., 2017; Mirata et al., 2022) and classified as a carcinogen for humans (class 1) by International Agency for Research on Cancer (IARC, 2012). For other minerals such as ferrierite (Gualtieri, 2018; Mattioli et al., 2022; Zoboli et al., 2019), mordenite (Di Giuseppe, 2020; Giordani, Ballirano, et al., 2022), offretite (Giordani et al., 2019; Mattioli et al., 2018), scolecite (Mattioli et al., 2016), mesolite and thomsonite (Betti et al., 2022; Giordani, Mattioli, et al., 2022), and others (e.g., fluoro-edenite, winchite, richterite, clay minerals; Gianfagna et al., 2003; NIOSH, 2011; Erskine & Bailey, 2018; Larson et al., 2016), the current knowledge does not permit an accurate risk classification. Exposure to mineral fibers represents a serious environmental hazard strictly correlated to fibrotic pulmonary diseases, pneumoconiosis, and various types of cancer in exposed subjects (Aust et al., 2011; Di Giuseppe et al., 2021; Gualtieri et al., 2017). Therefore, highlighting the effects of inhalable mineral fibers and the pathways involved in toxicity and carcinogenesis represents a fundamental step for carcinogenic/toxic fiber classification and for developing new preventive strategies. In general, fibers that rapidly dissolve or with a low biopersistence are assumed to have both a low toxicity and pathogenic potential (Gualtieri, 2018; Gualtieri et al., 2017). However, health effects resulting from exposure to soluble minerals could play an important role in pulmonary toxicity since it has been demonstrated that soluble carcinogens may pose a risk to both lungs and other organs (Bevan et al., 2018; Nemmar et al., 2002; Möller et al., 2008; WHO, 1999).

Among the soluble minerals, one of the most important is magnesium sulfate, present as natural epsomite or it can be found commercially as synthetic Epsom salt. Natural epsomite is a common hydrous magnesium sulfate with the general formula $Mg(SO_4)\cdot 7H_2O$ (Anthony et al., 1990; Giordani, Meli, et al., 2022). Natural epsomite occurs mainly on the walls of mines, caves, and outcrops of sulfide-bearing magnesian rocks (e.g., dolostone) but also as a product of evaporation at mineral springs and saline lakes, and rarely as fumarolic sublimate (Anthony et al., 1990; Biagioni et al., 2020). Epsom salt is widely used in many fields, and it has numerous medical and pharmaceutical applications, such as the treatment of cardiac arrhythmia, acute asthma, eclampsia, and gallstones (Ruiz-Agudo et al., 2007). Magnesium sulfate is also used as a constituent of drug formulations (Xia et al., 2016) and as a food additive (Joint FAO/WHO, 2007), but the same World Health Organization indicated that further toxicological studies and other information are required.

Since there are controversial opinions on inhalation of magnesium sulfate, here the effects of natural epsomite and its synthetic counterpart, Epsom salt, have been evaluated in an in vitro cell model which usually grows as a monocyte and, in appropriate conditions, differentiates into a macrophage. Macrophages seem involved in driving the antitumor response induced by mineral fibers since they represent the first defense against detrimental inhaled stimuli (Mirata et al., 2022). In this regard, several studies demonstrated that macrophages exposed to asbestos fibers undergo a frustrated phagocytosis (Hillegass et al., 2013; Ishida et al., 2019) that induces growth factor release and promotes tumor growth and development (Noy & Pollard, 2014).

In this study, the exposure to natural epsomite and Epsom salt has been investigated in monocytes and macrophages through morpho-functional and biochemical analyses to clarify and add additional information on soluble mineral effects on human health.

2 | MATERIALS AND METHODS

2.1 | Samples

Two different mineral samples were tested in this work. The first sample (Epsom salt) is a synthetic phase of pure magnesium sulfate (magnesium sulfate heptahydrate, Merck) and has been tested compared with natural epsomite. The second sample (epsomite crystals, named MP) is a natural fibrous magnesium sulfate collected in the Perticara mine (Rimini province, Italy) and described and characterized by Giordani, Meli, et al., (2022), Giordani et al., (2024). In this sample, a significant fraction of the fibers shows a very small size, and it is potentially inhalable for humans. Moreover, MP sample's calculated Aerodynamic Equivalent Diameter (Dae) is 5.1 μm. Accordingly, the MP fibers can easily penetrate and be deposited in the laryngeal and bronchial respiratory tract (Giordani, Meli, et al., 2022). The chemical composition of the MP sample is sulfur trioxides (32.93 wt%) and magnesium oxides (16.34 wt%); the water content, calculated by difference, is 50.73 wt %. It is worth noting that the MP sample contains a significant amount of radiogenic isotope ^{210}Po (about 5.5 Bq/g) and a minor amount of other trace elements (^{228}Th, Pb, As, Co, Fe, Mn, Ni, i, Sr, Ti, Zn) (Giordani et al., 2024; Giordani, Meli, et al., 2022).

2.2 | Environmental scanning electron microscopy

Morphological observations were performed using an environmental scanning electron microscope (ESEM) FEI Quanta 200 FEG (FEI, Hillsboro, OR, USA), equipped with an energy-dispersive x-ray spectrometer (EDS) for microchemical analyses. Operating conditions were 25 kV accelerating voltage, variable beam diameter, 10–12 mm working distance, and 0° tilt angle. The ESEM low vacuum mode was used, with a specimen chamber pressure set from 0.80 to 0.90 mbar. The images were obtained using a single-shot detector (SSD).

2.3 | Cell culture and treatments

U937 cell line is a human hematopoietic model established by a 39-year-old man with histiocytic lymphoma. These cells display

properties of immature monocytes and have been used as an in vitro model of macrophage. U937 cell line was grown in RPMI 1640, supplemented with 10% heat-inactivated fetal bovine serum, 2 mm glutamine and 1% antibiotics (Salucci et al., 2018). To differentiate monocytes into macrophages, the culture has been treated with 100 ng/mL Phorbol 12-Myristate 13-Acetate (PMA), a phorbol ester that regulates U937 cell adhesion molecules to attach to the flask surface and differentiate into a macrophage-like morphology (Otte et al., 2011).

Macrophages have been exposed to 10 or 20 nM Epsom salt or epsomite fibers for 24 or 48 h. Trypan Blue (TB) exclusion assay was performed to evaluate the number of living and dead cells in control conditions and in treated samples. Cell viability data have been obtained from 3 separate experiments and are furnished as mean ± SD. Paired T-Test Calculator has been used to compare control samples versus treated samples (Salucci et al., 2016) and data considered statistically significant (*) with p-value <.05 and highly statistically significant (**) with p-value <.001.

2.4 | Tem

Control and treated U937 cells were rinsed with PBS and immediately fixed in situ with 2.5% glutaraldehyde in 0.1 M phosphate buffer for 15 min. Macrophages, that grow adherent to the flasks, were gently scraped and centrifuged at 1200 rpm for 30 min in the same fixative (Codenotti et al., 2015). Both cell models were post-fixed in 1% OsO_4 in the same buffer (Giordano et al., 2019), dehydrated with ethanol and embedded in araldite (Salucci et al., 2016). Thin sections were collected on nickel grids and observed with TEM (FEI Italia SRL, Milano, Italy). To better identify their localization in the cells, and to exclude possible staining artifacts, some samples were observed without staining.

2.5 | Biochemical analyses: Electrophoresis and Western blotting

Levels of phosphorylated MAPKs in whole cell extracts from U937 cells (monocytes and macrophages) were determined by SDS-PAGE and Western blotting using phospho-specific antibodies as previously described. Samples (normalized for protein content before loading to 30 µg of protein) were resolved by 12% SDS-polyacrylamide gel electrophoresis (Laemmli, 1970). Pre-stained molecular- mass markers were run on adjacent lanes. The gels were electroblotted and stained with Coomassie Blue according to Towbin et al. (1979). Blots were probed with human recombinant specific anti-phospho-p38 and anti-phospho- ERK1/2 (1:1000) as primary antibodies, and horseradish- peroxidase-conjugated goat anti-rabbit IgG (1:3000) as a secondary antibody. Nitrocellulose membranes were stripped for 30 min at 50°C with stripping buffer (62.5 mM Tris–HCl, pH 6.7, containing 10 mM betamercaptoethanol and 2% SDS) and reprobed with anti-actin antibodies (1:1000) as loading controls. Immune complexes were visualized using an enhanced chemioluminescence Western blotting analysis system (Amersham Pharmacia Corp.) following the manufacturer's specifications. Western blot films were digitized (Chemidoc-Biorad) and band optical densities were quantified using a computerized imaging system (QuantityOne). Relative optical densities (arbitrary units) were normalized for the control band in each series.

3 | RESULTS

The morphological observation of the two investigated samples has been performed at ESEM. Epsom salt shows prismatic crystal morphologies ranging from 0.5 to 1 millimeter in size (Figure 1a). On the contrary, natural epsomite is composed of bundles of acicular fibrous crystals, with about 50 µm thick and variable lengths from 150 µm to few hundred µm (Figure 1b–d). Small single fibers and fibrils are also present, showing a rigid and fragile behavior or a curved and ductile one. Fibrils vary from less than 0.5 to 22 µm in width and from about 5 to 260 µm in length. Sometimes, very small particles of different chemical compositions are attached to fiber surfaces (Figure 1d). These impurities show a heterogeneous composition, in particular calcium sulfate (gypsum), Fe-sulfur (pyrite), native sulfur (S) and traces of Mn and Fe (probably related to the oxide mineral group) were detected. Differently to epsomite, the solubility of these phases is significantly lower in biological systems, and likely persist/accumulate longer.

The effect of these two compounds has been studied on U937 monocytes and macrophages, and cell response was evaluated at various dosages and after 24 h or 48 h from the exposition.

Cell viability, investigated through TB exclusion assay (that penetrates only in cells that do not have the intact plasma membrane and are, therefore, necrotic or in secondary necrosis), is about 96% for control monocytes. In monocytes, the Epsom salt effect can be considered negligible with a reduction in cell viability about of 15% after 48 h of treatment and at the highest dosage. Instead, after natural epsomite exposure a reduced monocyte viability can be observed, and it appears dose and time-dependent (Figure 2a). In particular, the number of dead cells thereby increases exposing the culture to the highest dosage and exposition time.

Morphological analysis (Figures 2 and 3) allows us to describe monocyte behavior after fiber administration. Control monocytes appear rounding with preserved subcellular organelles like mitochondria with well-organized cristae (Figure 2b,c). After Epsom salt exposure, swollen cells can be observed together with noticeable mitochondria bulge (Figure 2d,e), probably consequent of an osmotic alteration which rarely leads to necrotic death, confirming that osmotic shocking alone is relatively inefficient in cell disruption (Mantovanelli et al., 2021).

The insoluble fraction related to natural epsomite deeply penetrates in U937 cells, and its internalization into monocytes can be revealed starting from 24 h of treatment without significant cell damage (Figure 2f,g). The insoluble fraction appears largely

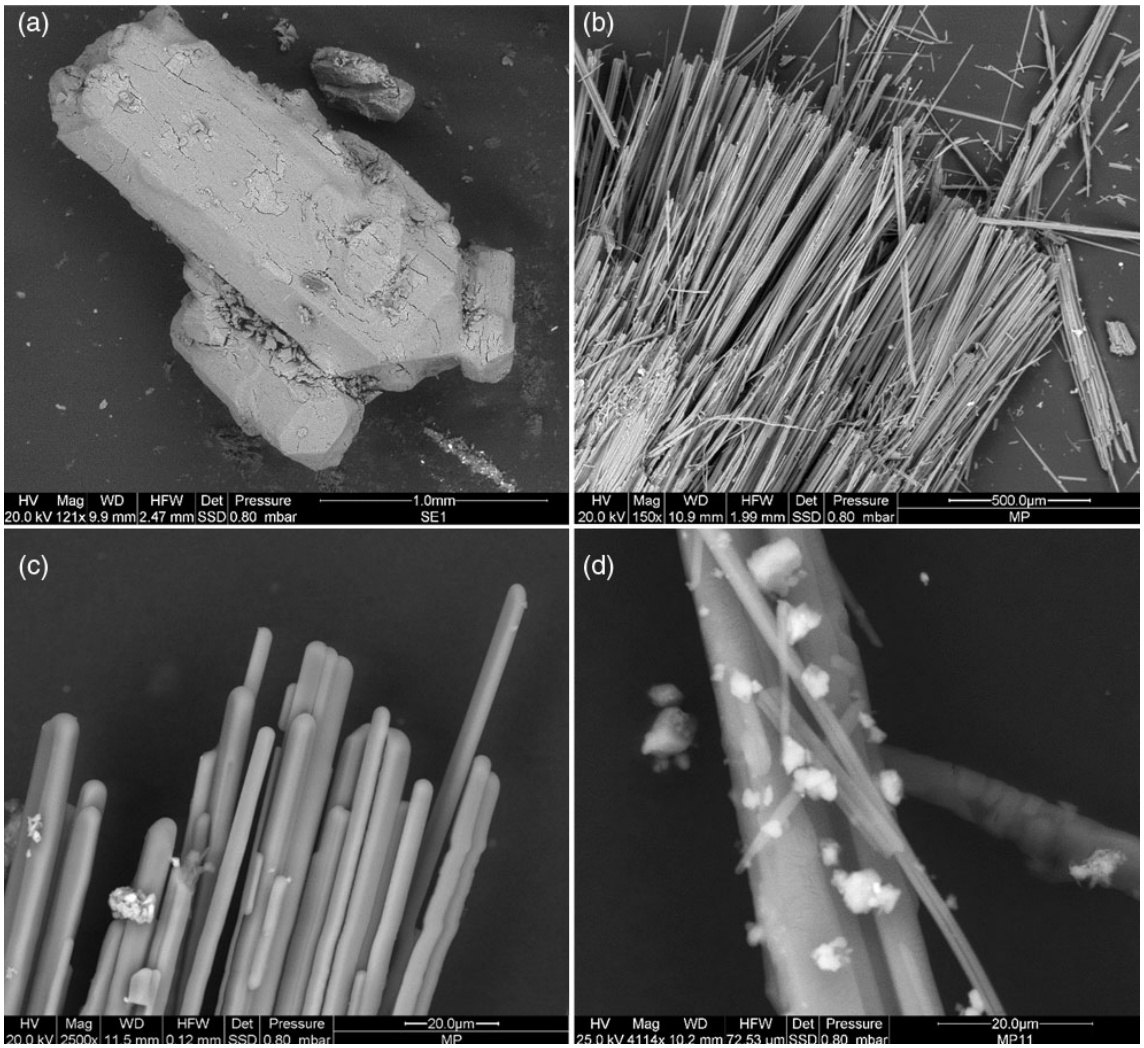

FIGURE 1 Environmental scanning electron microscope observations of Epsom salt (a) and natural epsomite fibers (b–d). Epsom salt shows prismatic crystal morphologies with sub-millimeter to millimeter size (a), while natural epsomite is composed of bundles of acicular to fibrous crystals about 50 µm thick (b–d).

internalized by some cells (Figure 2g,j) which show a diffuse microvillar component to form a concentric structure with the plasma membrane, to favor the entry of impurities inside the cell (Figure 2h,i). As shown in Figure 2h,j, some particulates form electron-dense circular structures sometimes englobed into vacuoles similar to lacunae.

After 48 h of Epsom salt administration, large subcellular organelles can be observed and only few monocytes appear degenerate (data not shown), a behavior similar to that of 24 h. Natural epsomite treatment at 48 h and at the highest dosage induces diffuse cell damage (Figure 3). In particular, an evident thickening of the nuclear envelope (not observable in control monocytes, Figure 3a), can be detected in some natural epsomite-treated cells (Figure 3b,c) which presented empty and altered mitochondria (Figure 3d) and features of secondary necrosis (Figure 3e,f).

Since monocytes after natural epsomite exposure show the presence of cell death, some cellular targets of the classical mitogen-activated protein kinase (MAPK) pathway, involved in the regulation of many cellular processes including inflammation, cell stress response, cell differentiation, cell division, cell proliferation have been investigated (Wang et al., 2012).

For that, U937 monocytes have been incubated with Epsom salt and natural epsomite for different periods of time. Control samples (untreated monocytes) were run in parallel. The phosphorylation state of MAPK p38 and ERK1/2 has been evaluated in monocyte protein extracts by electrophoresis and Western blotting with specific anti-phospho-MAPK antibodies and the results are reported in Figure 3. In monocytes incubated with Epsom salt (from 24 to 48 h) a smaller increase in the level of p-p38 (phosphorylated p38) MAPK was observed (Figure 3g). On the contrary in monocytes incubated with natural epsomite a rapid increase in the level of p-p38 has been detected (Figure 3g). Densitometric band analysis revealed that natural epsomite induced a significant increase in the level of p-p38 at 24 h (+60 and + 80% with respect to controls), followed by a

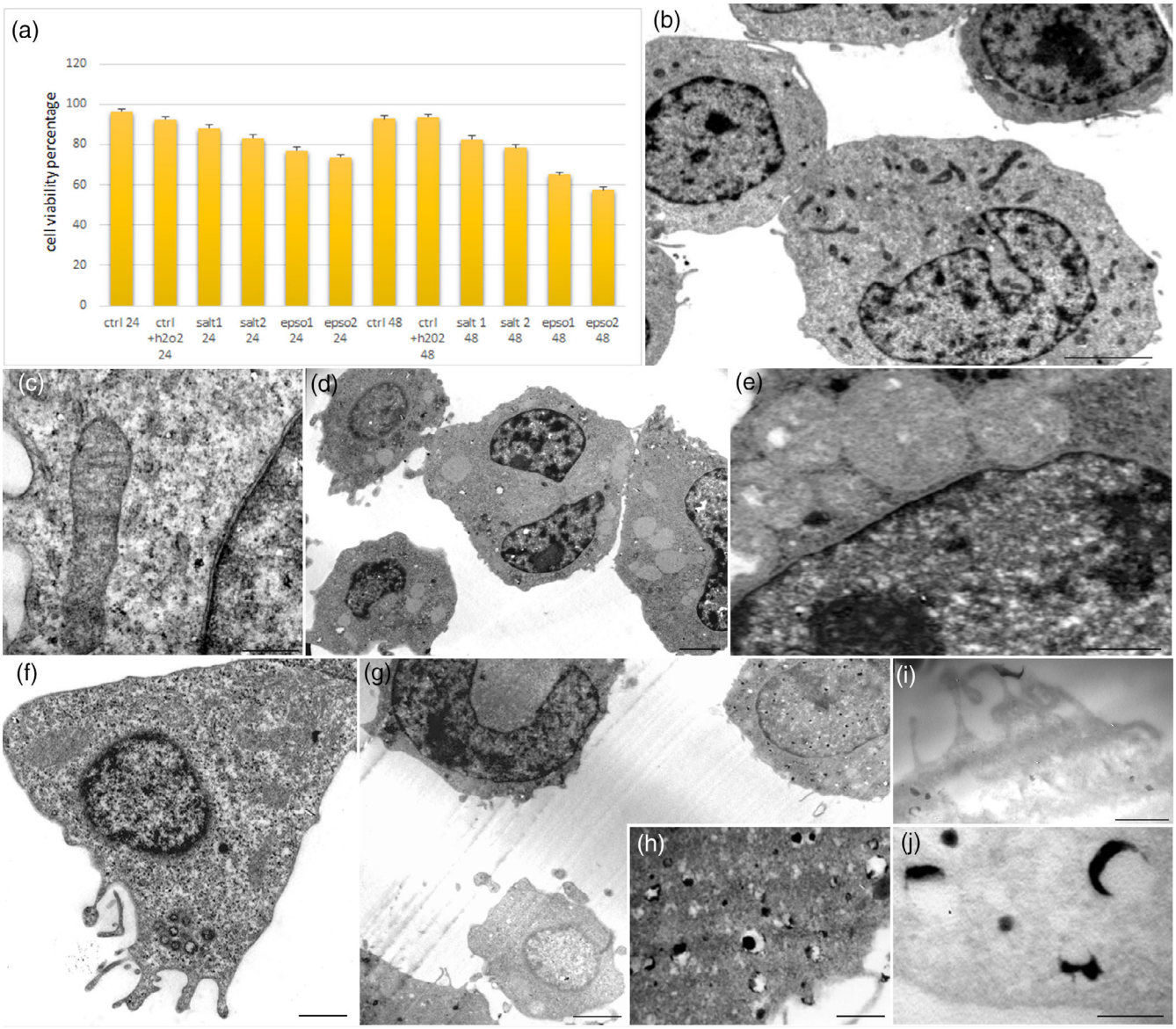

FIGURE 2 Cell viability percentage, $^{*}p < .05$, $^{**}p < .001$ (a). TEM micrographs of control cells (b,c), Epsom salt (d,e) and natural epsomite (f–i)—treated monocytes after 24 h of exposure and at 20 nM. Bars: 2 μm for (b,d,g); 1 μm for (e,f); 500 nm for (c,h); 200 nm for (j).

progressive decrease (+40 and + 25% at 48 h), while monocytes incubated with Epsom salt showed similar p38 phosphorylation levels to controls (Figure 3g). ERK1/2 (extracellular-signal-regulated kinase 1/2) MAPK recognized by anti-ERK MAPK antibodies as shown in Figure 3h. Monocytes incubated with Epsom salt showed a rapid and large increase in phosphorylation (+40 and +60% with respect to controls) in the level of p-ERK1/2 (phosphorylated ERK1/2). Natural epsomite induced a smaller decrease in ERK1/2 MAPK phosphorylation from 24 h; such a decrease was transient and followed by a return to control levels at 48 h (Figure 3h).

Successively, monocytes have been differentiated into macrophages and the effects of Epsom salt or natural epsomite fibers have been investigated at the same dosages and time points considered for undifferentiated culture.

Macrophage response monitored through TB assay revealed the same cell behavior described for monocytes as appeared in the graph in Figure 4a. Therefore, Epsom salt induces a weak cell death which slightly raises with increasing dose and treatment time. After natural epsomite administration, a certain number of cells appear dead, and at the highest dosage and exposure time the death is about 40% with respect to the control condition (Figure 4a).

Ultrastructural analysis (Figure 4) allows us to describe control macrophage morphology characterized by a large cell size with numerous cytoplasmic vacuoles suggestive of lysosomes, which contain ingested cellular and noncellular material in different stages of degradation (Figure 4b,c).

Macrophages exposed to Epsom salt showed a morphology like control cells with large and diffuse cytoplasmic vacuoles but with

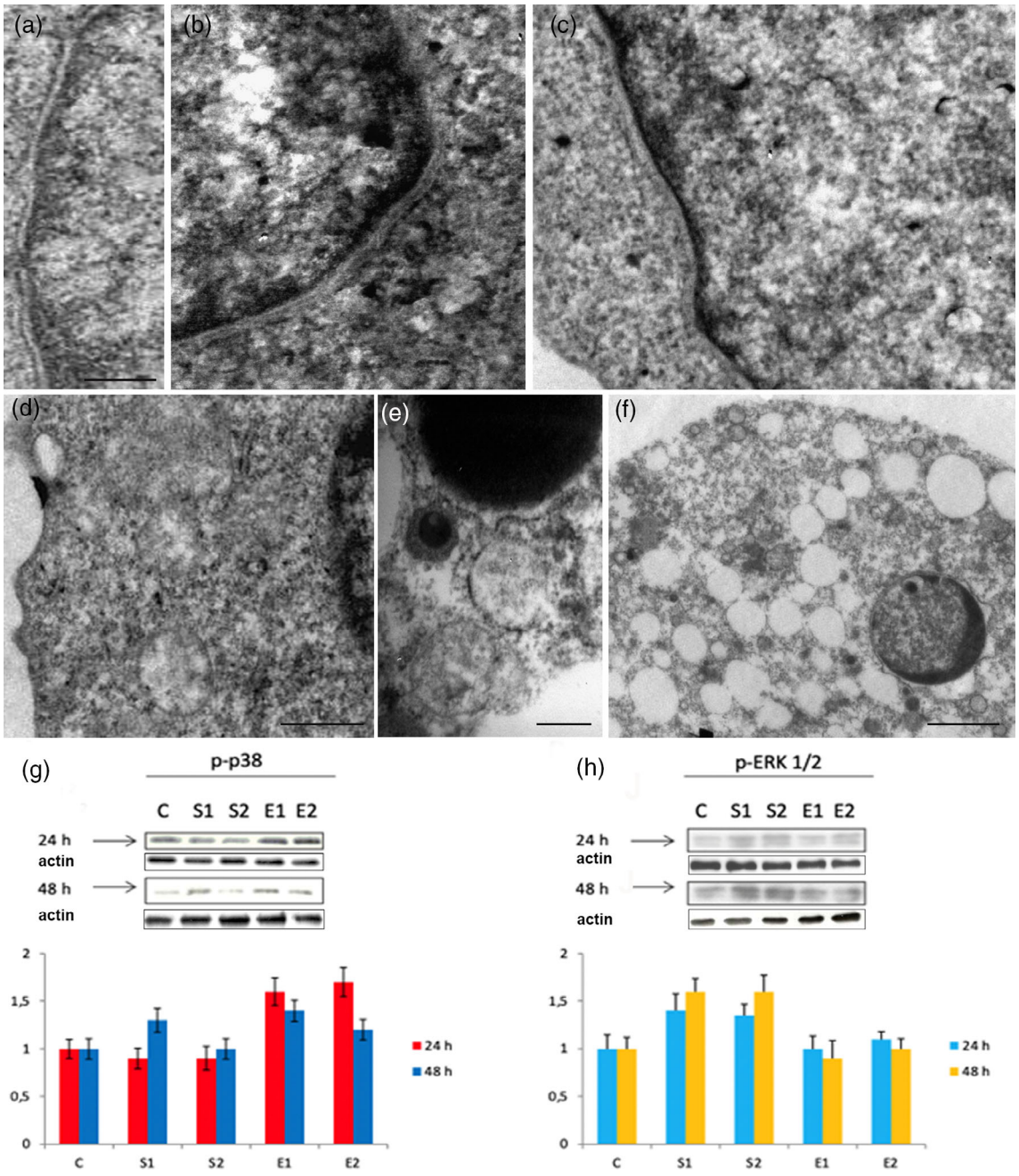

FIGURE 3 TEM micrographs of the control condition (a) and monocytes after 48 h of natural epsomite treatment (b–f) at 10 nM (b–d) or 20 nM (e,f) dose of exposure. Natural epsomite induces thickening of the nuclear membrane (b,c) compared to the control cell (a). Furthermore, mitochondria alterations (d) and cells in secondary necrosis (e,f) can be observed in natural epsomite-treated samples. In (g) (left panel), a representative blot of p38 MAPK phosphorylation in control monocytes was incubated with Epsom salt and natural epsomite at 24–48 h. Lower panels: densitometric analysis of blots from three independent experiments (means ± S.D.). In (h) (right panel) a representative blot of ERK1/2 MAPK phosphorylation in control monocytes incubated with Epsom salt and natural epsomite at 24–48 h. Lower panels: densitometric analysis of blots from three independent experiments (means ± S.D.). Bars: 200 nm for (a–c) (bar in a) and (e); 1 μm for (d) and 2 μm for (f).

preserved mitochondria (Figure 4d,e), even if, sometimes, few cells in necrosis can be observed.

After natural epsomite exposure, macrophages show a preserved morphology with large aqueous vacuoles together with a certain number of degradative vacuoles (Figure 4f,g). Small and large residual fragments (Figure 4f–l) appear internalized into cells thanks to their elongated arms or pseudopods increasing surface area for antigen uptake (Figure 4h). Small particles are phagocytized and degraded from cells through the lysosomal system (Figure 4g). On the contrary, great, and elongated impurities, even if some of them internalized into vacuoles (Figure 4i), cause at the highest dose and time of exposure, an impairment in the

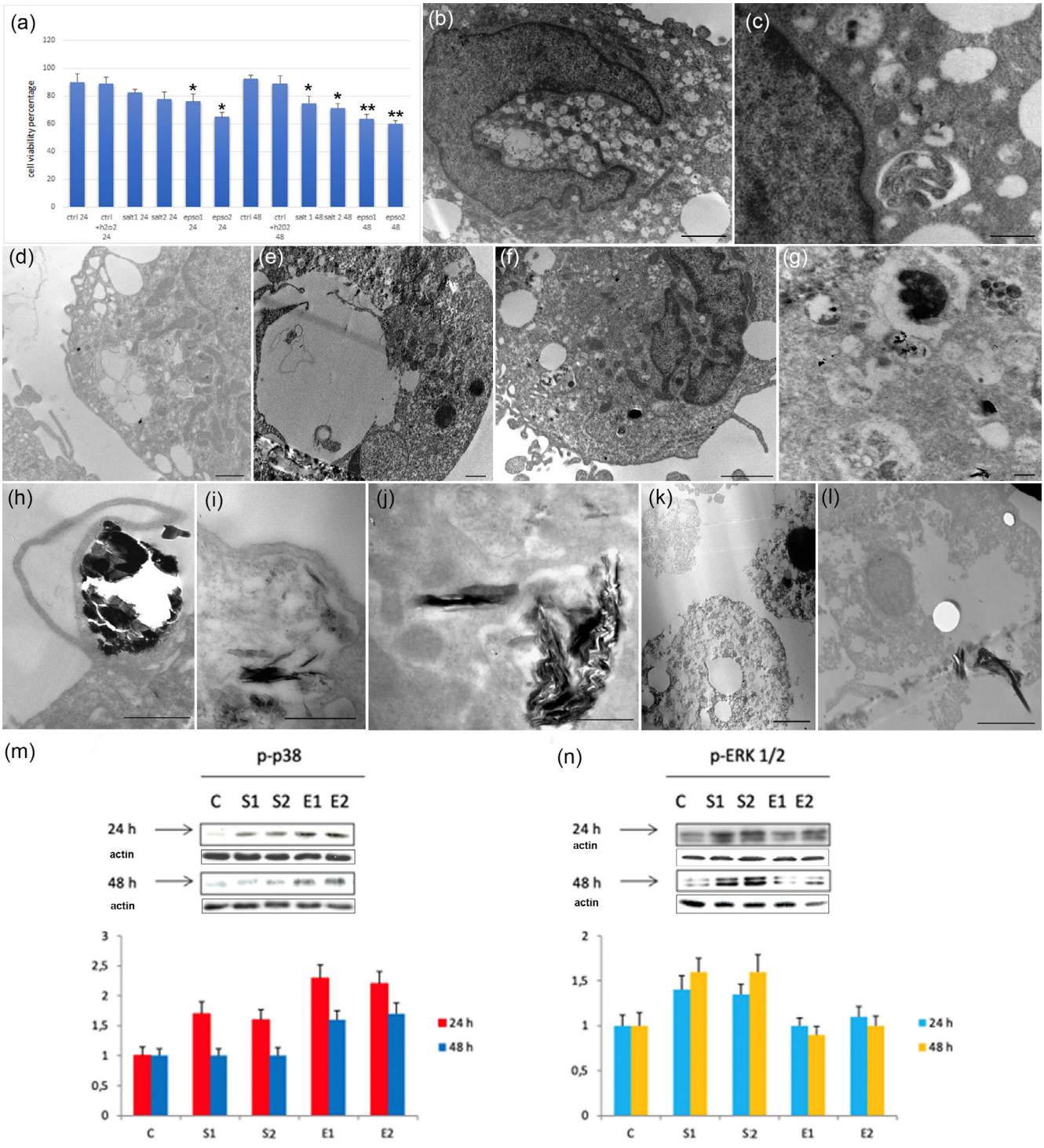

FIGURE 4 Cell viability percentage, $^{*}p < .05$, $^{**}p < .001$ (a). TEM micrographs of control macrophages (b,c) and Epsom salt (d,e) or natural epsomite (f–l)—treated cells after 24 h (d,f–j) or 48 (e,k,l) at the highest fiber dosage. In (m) (left panel), a representative blot of p38 MAPK phosphorylation in control macrophages was incubated with Epsom salt and natural epsomite at 24–48 h. Lower panels: densitometric analysis of blots from three independent experiments (means ± S.D.) In (n) (right panel) a representative blot of ERK1/2 MAPK phosphorylation in control macrophages incubated with Salt and Epsomite at 24–48 h. Lower panels: densitometric analysis of blots from three independent experiments (means ± S.D.). Bars: 2 μm for (b,f–h,k and l); 1 μm for (c–e,k); 500 nm for (a,g,i,j).

degradative processes which results in the macrophagic necrotic death (Figure 4k,l).

MAPKs phosphorylation has been evaluated in macrophages incubated with Epsom salt and natural epsomite too (Figure 4m,n). Epsom salt-induced a significant increase in the level of p-p38 at 24 h (+50% with respect to controls), followed by a progressive decrease to control values at 48 h (Figure 4m). Macrophages incubated with Epsom salt showed a rapid and large increase in phosphorylation

(+ 50 and + 70% with respect to controls) in the level of p-ERK1/2 (phosphorylated ERK1/2). The phosphorylation level of MAPK ERK1/2 was persistent and significant at all time incubation times (Figure 4n). Natural epsomite induced a rapid, dramatic and persistent increase in the level of p-p38 with respect to controls at all times of incubation (Figure 4m). Natural epsomite also induced a smaller increase in ERK1/2 MAPK phosphorylation from 24 h; such a decrease was transient and followed by a return to control levels at 48 h (Figure 4m).

4 | CONCLUSIONS

Lung cancer studies have indicated that mineral fiber exposure may be a serious hazard to cancer development (Strurm, 2010). Extensive investigations have demonstrated that inhalation of absestos fibers leads to malignant transformation of bronchial and alveolar epithelial cells (Gazzano et al., 2023; Kamp, 2009; Liu et al., 2010). If asbestos-related lung disease is extensively investigated on different lung cell types, the effect of particulates and fibers with high solubility in water and/or in biological environments appears scarcely detailed in biological systems. However, recently, scientists' interest in fibrous minerals has significantly increased since some particulates could be potentially dangerous to human health These studies on inhaled minerals are preferentially performed on macrophages or fibroblasts, two phenotypes known for mediating fibrosis, the first cell type involved in inflammation modulation, and the second one in maintaining the extracellular matrix (Mirata et al., 2022; Yu et al., 2021). Here, the effects of the water-soluble natural epsomite fibers as well as of synthetic counterpart Epsom salt were investigated in an in vitro U937 model both at the undifferentiated and differentiated stage and using morpho-functional and biochemical approaches. The ultrastructural analyses reveal that cells exposed to Epsom salt undergo an osmotic shock characterized by dilatation of a certain number of subcellular organelles. However, this osmotic perturbation does not cause irreversible damage as confirmed by biochemical data which demonstrate MAPK activation when cells were treated with Epsom salt. In fact, p38 appears slightly increased at 24 h and its expression is reduced and comparable to that of the control condition after 48 h of treatment. As known, p38 is a stress response kinase that negatively regulates cell cycle progression at both the G1/S and G2/M transition phases by downregulation of cyclins and upregulation of CDK inhibitors (Liu et al., 2022). For instance, p38 activation regulates osmo-stress-induced apoptosis in Xenopus oocytes and its up-regulation accelerates cytochrome c release and caspase-3 activation (Messaoud et al., 2015). In Epsom salt treated-monocytes p38 rapidly increases to respond to osmotic perturbation but its expression level return to a physiological level after 48 h, suggesting that Epsom salt does not lead to monocyte death. This scenario appears confirmed by the behavior of another MAPK kinase, that is, ERK. ERK activation induces various cellular responses including cell survival, cell growth, cell metabolism, cell migration and cell differentiation (Lavoie et al., 2020). In salt-treated samples, p-ERK appears upregulated suggesting its crucial role in promoting a survival response. In fact, it is known that ERK activation is involved in apoptosis inhibition, particularly concerning the intrinsic pathway (Edlich, 2018; Kale et al., 2018). On the contrary, natural epsomite fiber exposure induces progressive cell damage and some monocytes after 48 h of treatment show a thickening of the nuclear membrane and features of secondary necrosis. This is confirmed by the rapid p38 upregulation followed by p-ERK levels similar to those of the control condition, suggesting that some monocytes are going to die.

Moreover, macrophages exposed to natural epsomite showed residual fraction internalization leading to the engulfment of the phagocytosis processes and necrotic cell death. Biochemical analysis evidences a p38 upregulation both at 24 and 48 h and this behavior, also confirmed by the reduced p-ERK expression, correlates with cellular damage and a necrotic fate. Therefore, the basal level of ERK is insufficient to promote both monocyte and macrophage survival after natural epsomite treatment, confirming the crucial role of this kinase in the regulation of cellular homeostasis (Lavoie et al., 2020) and, so, suggesting the involvement of a potential inflammatory pathway to longer treatment times.

In conclusion, if Epsom salt can be considered not toxic at the tested concentrations and on the selected cell line, chronic exposition to the tested natural epsomite fibers can irreversibly perturbate U937 cellular homeostasis leading to necrotic cell death. Considering the similar general formula of the two tested samples (i.e., magnesium sulphate heptahydrate), we need to take into account that a crucial role on the cellular toxicity effect could be played by mineralogical impurities (despite being very scarce) and the presence of toxic/radioactive elements detected in the natural sample. On the other hand, natural samples always contain a certain degree of impurities, which in terms of etiology can be crucial for the development of health problems.

These findings open a new scenario on the dangerousness of epsomite fibers on relevant human in vitro cell models, thus adding crucial information on this mineral that could be potentially hazardous for human health.

AUTHOR CONTRIBUTIONS

Sara Salucci: Writing – original draft; writing – review and editing; investigation; data curation; conceptualization; validation. **Matteo Giordani:** Supervision; writing – review and editing; data curation. **Michele Betti:** Methodology; supervision; data curation. **Laura Valentini:** Data curation; supervision. **Pietro Gobbi:** Supervision; conceptualization. **Michele Mattioli:** Funding acquisition; writing – review and editing; data curation; supervision.

ACKNOWLEDGMENTS

Thanks to "Museo Sulfur" of Perticara (RN) for its kind hospitality to the author (MG) and logistic support during the sampling phase. The authors thank dr D. Burini for her scientific and technical support.

FUNDING INFORMATION

PRIN 2017 This research was conducted under the project "Fibers a Multidisciplinary Mineralogical, Crystal-Chemical and Biological

Project to Amend the Paradigm of Toxicity and Cancerogenicity of Mineral Fibers" (PRIN: PROGETTI DI RICERCA DI RILEVANTE INTERESSE NAZIONALE-Bando 2017-Prot. 20173X8WA4).

DATA AVAILABILITY STATEMENT

The data that support the findings of this study are available from the corresponding author upon reasonable request.

REFERENCES

Anthony, J. W., Bideaux, R. A., Bladh, K. W., & Nichols, M. C. (1990). *Elements, sulfides. Sulfosalts* (Vol. 1 (of handbook of mineralogy)). Mineral data publishing.

Aust, A. E., Cook, P. M., & Dodson, R. D. (2011). Morphological and chemical mechanisms of elongated mineral particle toxicities. *Journal of Toxicology and Environmental Health, Part B: Critical Reviews*, *14*, 40–75. https://doi.org/10.1080/10937404.2011.556046

Betti, M., Nasoni, M. G., Luchetti, F., Giordani, M., & Mattioli, M. (2022). Potential toxicity of natural fibrous zeolites: In vitro study using Jurkat and HT22 cell lines. *Minerals*, *12*, 988. https://doi.org/10.3390/min12080988

Bevan, R. J., Kreiling, R., Levy, L. S., & Warheit, D. B. (2018). Toxicity testing of poorly soluble particles, lung overload and lung cancer. *Regulatory Toxicology and Pharmacology*, *100*, 80–91.

Biagioni, C., Mauro, D., & Pasero, M. (2020). Sulfates from the pyrite ore deposits of the Apuan Alps (Tuscany, Italy): A review. *Minerals*, *10*, 1092. https://doi.org/10.3390/min10121092

Cangiotti, M., Battistelli, M., Salucci, S., Falcieri, E., Mattioli, M., Giordani, M., & Ottaviani, M. F. (2017). Electron paramagnetic resonance and transmission electron microscopy study of the interactions between asbestiform zeolite fibers and model membranes. *Journal of Toxicology and Environmental Health. Part A*, *80*, 171–187. https://doi.org/10.1080/15287394.2016.1275901

Cangiotti, M., Salucci, S., Battistelli, M., Falcieri, E., Mattioli, M., Giordani, M., & Ottaviani, M. F. (2018). EPR, TEM and cell viability study of asbestiform zeolite fibers in cell media. *Colloids and Surfaces B: Biointerfaces*, *161*, 147–155. https://doi.org/10.1016/j.colsurfb.2017.10.045

Codenotti, S., Battistelli, M., Burattini, S., Salucci, S., Falcieri, E., Rezzani, R., Faggi, F., Colombi, M., Monti, E., & Fanzani, A. (2015). Melatonin decreases cell proliferation, impairs myogenic differentiation and triggers apoptotic cell death in rhabdomyosarcoma cell lines. *Oncology Reports*, *34*, 279–287.

Di Giuseppe, D. (2020). Characterization of fibrous Mordenite: A first step for the evaluation of its potential toxicity. *Crystals*, *10*, 769. https://doi.org/10.3390/cryst10090769

Di Giuseppe, D., Scarfì, S., Alessandrini, A., Bassi, A. M., Mirata, S., Almonti, V., Ragazzini, G., Mescola, A., Filaferro, M., Avallone, R., Vitale, G., Scognamiglio, V., & Gualtieri, A. F. (2021). Acute cytotoxicity of mineral fibres observed by time-lapse video microscopy. *Toxicology*, *466*, 153081. https://doi.org/10.1016/j.tox.2021.153081

Edlich, F. (2018). BCL-2 proteins and apoptosis: Recent insights and unknowns. *Biochemical and Biophysical Research Communications*, *500*, 26–34.

Erskine, B. G., & Bailey, M. (2018). Characterization of asbestiform glaucophane-winchite in the franciscan complex blueschist, northern diablo range, California. *Toxicology and Applied Pharmacology*, *361*, 3–13.

Gazzano, E., Petriglieri, J. R., Aldieri, E., Fubini, B., Laporte-Magoni, C., Pavan, C., Tomatis, M., & Turci, F. (2023). Cytotoxicity of fibrous antigorite from New Caledonia. *Environmental Research*, *230*, 115046.

Gianfagna, A., Ballirano, P., Bellatreccia, F., Bruni, B., Paoletti, L., & Oberti, R. (2003). Characterization of amphibole fibres linked to mesothelioma in the area of Biancavilla, eastern Sicily, Italy. *Mineralogical Magazine*, *67*, 1221–1229. https://doi.org/10.1180/0026461036760160

Giordani, M., Ballirano, P., Pacella, A., Meli, M. A., Roselli, C., Di Lorenzo, F., Fagiolino, I., & Mattioli, M. (2022). Another potentially hazardous zeolite from northern Italy: Fibrous Mordenite. *Minerals*, *12*, 627. https://doi.org/10.3390/min12050627

Giordani, M., Cametti, G., Di Lorenzo, F., & Churakov, S. V. (2019). Real-time observation of fibrous zeolites reactivity in contact with simulated lung fluids (SLFs) obtained by atomic force microscope (AFM). *Minerals*, *9*, 83. https://doi.org/10.3390/min9020083

Giordani, M., Mattioli, M., Cangiotti, M., Fattori, A., Ottaviani, M. F., Betti, M., Ballirano, P., Pacella, A., Di Giuseppe, D., Scognamiglio, V., & Hanuskova, M. (2022). Characterisation of potentially toxic natural fibrous zeolites by means of electron paramagnetic resonance spectroscopy and morphological-mineralogical studies. *Chemosphere*, *291*, 133067. https://doi.org/10.1016/j.chemosphere.2021.133067

Giordani, M., Meli, M. A., Roselli, C., Betti, M., Peruzzi, F., Taussi, M., Valentini, L., Fagiolino, I., & Mattioli, M. (2022). Could soluble minerals be hazardous to human health? Evidence from fibrous epsomite. *Environmental Research*, *206*, 112579. https://doi.org/10.1016/j.envr.2021.112579

Giordani, M., Taussi, M., Meli, M. A., Roselli, C., Zambelli, G., Fagiolino, I., & Mattioli, M. (2024). High-levels of toxic elements and radioactivity in an abandoned Sulphur mine: Insights on the origin and associated environmental concerns. *Science of the Total Environment*, *906*, 167498. https://doi.org/10.1016/j.scitotenv.2023.167498

Giordano, F. M., Burattini, S., Buontempo, F., Canonico, B., Martelli, A. M., Papa, S., Sampaolesi, M., Falcieri, E., & Salucci, S. (2019). Diet modulation restores Autophagic flux in damaged skeletal muscle cells. *The Journal of Nutrition, Health & Aging*, *23*, 739–745.

Gualtieri, A. F. (2018). Towards a quantitative model to predict the toxicity/pathogenicity potential of mineral fibers. *Toxicology and Applied Pharmacology*, *361*, 89–98. https://doi.org/10.1016/j.taap.2018.05.012

Gualtieri, A. F., Mossman, B. T., & Roggli, V. L. (2017). Towards a general model to predict the toxicity and pathogenicity of mineral fibres mineral Fibres: Crystal chemistry, chemical-physical properties. *Biological Interaction and Toxicity: European Mineralogical Union–EMU Notes in Mineralogy*, *18*, 501–532. (Chapter 15).

Gualtieri, A. F. (2023). Journey to the centre of the lung. The perspective of a mineralogist on the carcinogenic effects of mineral fibres in the lungs. *Journal of Hazardous Materials*, *442*, 130077.

Hillegass, J. M., Miller, J. M., MacPherson, M. B., Westbom, C. M., Sayan, M., Thompson, J. K., Macura, S. L., Perkins, T. N., Beuschel, S. L., Alexeeva, V., Pass, H. I., Steele, C., Mossman, B. T., & Shukla, A. (2013). Asbestos and erionite prime and activate the NLRP3 inflammasome that stimulates autocrine cytokine release in human mesothelial cells. *Particle and Fibre Toxicology*, *10*, 39. https://doi.org/10.1186/1743-8977-10-39

IARC. (2012). Asbestos (chrysotile, amosite, crocidolite, tremolite, actinolite and anthophyllite), Arsenic, Metals, Fibres and Dusts. *International Agency for Research on Cancer*.

Ishida, T., Fujihara, N., Nishimura, T., Funabashi, H., Hirota, R., Ikeda, T., & Kuroda, A. (2019). Live-cell imaging of macrophage phagocytosis of asbestos fibers under fluorescence microscopy. *Genes and Environment*, *41*, 14. https://doi.org/10.1186/s41021-019-0129-4

Joint FAO/WHO Expert Committee on Food Additives. Meeting (67th, 2006, Rome, Italy), World Health Organization & Food and Agriculture Organization of the United Nations. (2007). *Evaluation of certain food additives and contaminants: sixty-seventh report of the joint FAO/WHO expert committee on food additives*. World Health Organization.

Kale, J., Osterlund, E. J., & Andrews, D. W. (2018). BCL-2 family proteins: Changing partners in the dance towards death. *Cell Death and Differentiation*, *25*, 65–80.

Kamp, D. W. (2009). Asbestos-induced lung diseases: An update. *Translational Research*, *153*, 143–152.

Laemmli, U. K. (1970). Cleavage of structural proteins during the assembly of the head of bacteriophage T4. *Nature*, *227*, 680–685. https://doi.org/10.1038/227680a0

Larson, D., Powers, A., Ambrosi, J. P., Tanji, M., Napolitano, A., Flores, E. G., Baumann, F., Pellegrini, L., Jennings, C. J., Buck, B. J., & McLaurin, B. T. (2016). Investigating palygorskite's role in the development of mesothelioma in southern Nevada: Insights into fiber-induced carcinogenicity. *Journal of Toxicology and Environmental Health, Part B*, *19*, 213–230. https://doi.org/10.1080/10937404.2016.1195321

Lavoie, H., Gagnon, J., & Therrien, M. (2020). ERK signaling: A master regulator of cell behaviour, life and fate. *Nature Reviews Molecular Cell Biology*, *21*, 607–632.

Liu, G., Beri, R., Mueller, A., & Kamp, D. W. (2010). Molecular mechanisms of asbestos-induced lung epithelial cell apoptosis. *Chemico-Biological Interactions*, *188*, 309–318.

Liu, Z., Demian, W., Persaud, A., Jiang, C., Subramanaya, A. R., & Rotin, D. (2022). Regulation of the p38-MAPK pathway by hyperosmolarity and by WNK kinases. *Scientific Reports*, *12*, 14480.

Mantovanelli, L., Gaastra, B. F., & Poolman, B. (2021). Fluorescence-based sensing of the bioenergetic and physicochemical status of the cell. *Current Topics in Membranes*, *88*, 1–54. https://doi.org/10.1016/bs.ctm.2021.10.002

Mattioli, M., Ballirano, P., Pacella, A., Cangiotti, M., Di Lorenzo, F., Valentini, L., Meli, M. A., Roselli, C., Fagiolino, I., & Giordani, M. (2022). Fibrous Ferrierite from northern Italy: Mineralogical characterization, surface properties, and assessment of potential toxicity. *Minerals*, *12*, 626. https://doi.org/10.3390/min12050626

Mattioli, M., Giordani, M., Arcangeli, P., Valentini, L., Boscardin, M., Pacella, A., & Ballirano, P. (2018). Prismatic to asbestiform offretite from northern Italy: Occurrence, morphology and crystal-chemistry of a new potentially hazardous zeolite. *Minerals*, *8*, *69*. https://doi.org/10.3390/min8020069

Mattioli, M., Giordani, M., Dogan, M., Cangiotti, M., Avella, G., Giorgi, R., Dogan, A. U., & Ottaviani, M. F. (2016). Morpho-chemical characterization and surface properties of carcinogenic zeolite fibers. *Journal of Hazardous Materials*, *306*, 140–148. https://doi.org/10.1016/j.jhazmat.2015.11.015

Messaoud, N. B., Katzarova, I., & López, J. M. (2015). Basic properties of the p38 signaling pathway in response to hyperosmotic shock. *PLoS One*, *10*, e0135249.

Mirata, S., Almonti, V., Di Giuseppe, D., Fornasini, L., Raneri, S., Vernazza, S., Bersani, D., Gualtieri, A. F., Bassi, A. M., & Scarfì, S. (2022). The acute toxicity of mineral Fibres: A systematic in vitro study using different THP-1 macrophage phenotypes. *International Journal of Molecular Sciences*, *23*, 2840. https://doi.org/10.3390/ijms23052840

Möller, W., Felten, K., Sommerer, K., Scheuch, G., Meyer, G., Meyer, P., Haussinger, K., & Kreyling, W. G. (2008). Deposition, retention, and translocation of ultrafine particles from the central airways and lung peripheryAm. *Journal of Respiratory and Critical Care Medicine*, *177*, 426–432.

National Institute for Occupational Safety and Health (NIOSH). (2011). Asbestos fibers and other elongate mineral particles: State of the science and roadmap for research. In *Current intelligence bulletin 62, version 4*. Cincinnati, OH, USA.

Nemmar, A., Hoet, P. M., Vanquickenborne, B., Dinsdale, D., Thomeer, M., Hoylaerts, M. F., Vanbilloen, H., Mortelmans, L., & Nemery, B. (2002). Passage of inhaled particles into the blood circulation in humans. *Circulation*, *105*, 411–414.

Noy, R., & Pollard, J. W. (2014). Tumor-associated macrophages: From mechanisms to therapy. *Immunity*, *41*, 49–61.

Otte, A., Mandel, K., Reinstrom, G., & Hass, R. (2011). Abolished adherence alters signaling pathways in phorbol ester-induced human U937 cells. *Cell Communication and Signaling: CCS*, *9*, 20.

Ruiz-Agudo, E., Martín-Ramos, J. D., & Rodriguez-Navarro, C. (2007). Mechanism and kinetics of dehydration of epsomite crystals formed in the presence of organic additives. *The Journal of Physical Chemistry. B*, *111*, 41–52. https://doi.org/10.1021/jp064460b

Salucci, S., Baldassarri, V., Canonico, B., Burattini, S., Battistelli, M., Guescini, M., Papa, S., Stocchi, V., & Falcieri, E. (2016). Melatonin behavior in restoring chemical damaged C2C12 myoblasts. *Microscopy Research and Technique*, *79*, 532–540.

Salucci, S., Burattini, S., Buontempo, F., Orsini, E., Furiassi, L., Mari, M., Lucarini, S., Martelli, A. M., & Falcieri, E. (2018). Marine bisindole alkaloid: A potential apoptotic inducer in human cancer cells. *European Journal of Histochemistry*, *62*, 2881.

Strurm, R. (2010). Theoretical approach to the hit probability of lung-cancer-sensitive epithelial cells by mineral fibers with various aspect ratios thorac cancer. *Thoracic Cancer*, *1*, 116–125.

Thompson, J. K., MacPherson, M. B., Beuschel, S. L., & Shukla, A. (2017). Asbestos-induced mesothelial to fibroblastic transition is modulated by the inflammasome. *The American Journal of Pathology*, *187*, 66.

Towbin, H., Staehelin, T., & Gordon, J. (1979). Electrophoretic transfer of proteins from polyacrylamide gels to nitrocellulose sheets: procedure and some applications. *Proceedings of the National Academy of Sciences of the United States of America*, *76*, 4350–4354. https://doi.org/10.1073/pnas.76.9.4350

Wang, S. N., Lee, K. T., Tsai, C. J., Chen, Y. J., & Yeh, Y. T. (2012). Phosphorylated p38 and JNK MAPK proteins in hepatocellular carcinoma. *European Journal of Clinical Investigation*, *2012*(42), 1295–1301. https://doi.org/10.1111/eci.12003

World Health Organization (WHO). (1986). *Asbestos and other natural mineral fibers*; Environmental health criteria, 53 (pp. 69–107). World Health Organization (WHO).

World Health Organization (WHO). (1999). Occupational and environmental health team. Hazard prevention and control in the work environment. Report WHO/SDE/OEH/99.14, Geneva.

Xia, Y., Bo, A., Liu, Z., Chi, B., Su, Z., Hu, Y., Luo, R., Su, X., & Sun, J. (2016). Effects of magnesiumsulfate on apoptosis in cultured human gastric epithelial cells. *Food and Agricultural Immunology*, *27*, 171–181.

Yu, S. H., Kumar, M., Kim, I. W., Rimer, J. D., & Kim, T. J. (2021). A comparative analysis of in vitro toxicity of synthetic zeolites on IMR-90 human lung fibroblast cells molecules. 26, 3194.

Zoboli, A., Di Giuseppe, D., Baraldi, C., Gamberini, M. C., Malferrari, D., Urso, G., Gualtieri, M. L., Bailey, M., & Gualtieri, A. F. (2019). Characterisation of fibrous ferrierite in the rhyolitic tuffs at lovelock, Nevada, USA. *Mineralogical Magazine*, *83*, 577–586.

How to cite this article: Salucci, S., Giordani, M., Betti, M., Valentini, L., Gobbi, P., & Mattioli, M. (2023). The in vitro cytotoxic effects of natural (fibrous epsomite crystals) and synthetic (Epsom salt) magnesium sulfate. *Microscopy Research and Technique*, 1–10. https://doi.org/10.1002/jemt.24458